Supporting Information

Hierarchical Ti_3C_2@TiO_2 MXene Hybrids with Controllable Interlayer Distance for High Durable Lithium-ion Batteries

Li Li,*[a,c] Gaoxue Jiang,[a] Cuihua An,*[b,c] Zhengjun Xie,[a] Yijing Wang,*[c] Lifang Jiao,[c] Huatang Yuan,[c]

[a]School of Materials Science and Engineering, University of Jinan, Jinan 250022, Shandong, China

[b]Tianjin Key Laboratory of Advanced Functional Porous Materials, Institute for New Energy Materials & Low-Carbon Technologies, School of Materials Science and Engineering, Tianjin University of Technology, Tianjin 300384, China

[c]Key Laboratory of Advanced Energy Materials Chemistry (Ministry of Education), College of Chemistry, Nankai University, Tianjin 300071, China

* *E-mail addresses*: mse_lil@ujn.edu.cn (L. Li), wangyj@nankai.edu.cn (Y. Wang)

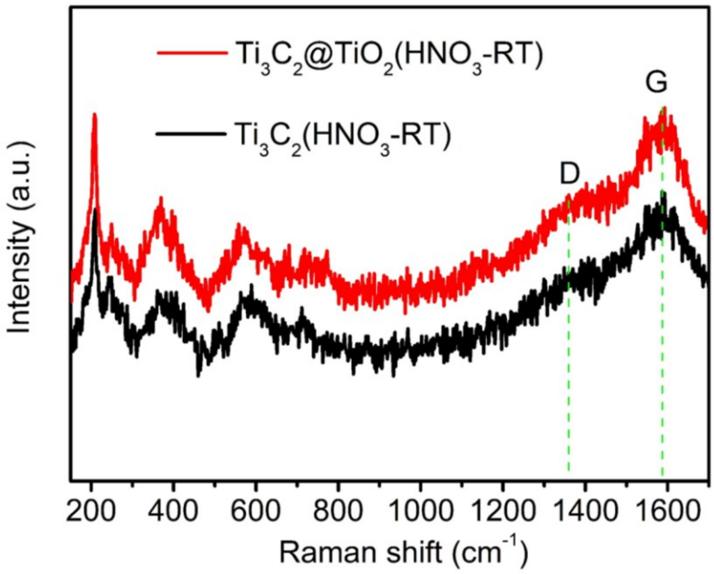

Fig. S1. Raman spectra of Ti_3C_2(HNO_3-RT) and Ti_3C_2@TiO_2(HNO_3-RT) hybrids.

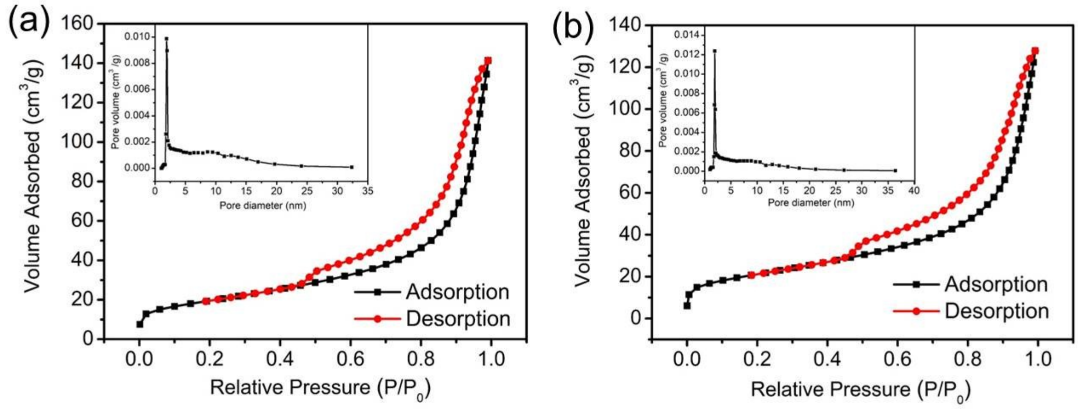

Fig. S2. N_2 adsorption/desorption isotherms of Ti_3C_2(HNO_3-RT) (a) and Ti_3C_2@TiO_2(HNO_3-RT) (b), respectively. The inserts images are the corresponding pore size distributions.

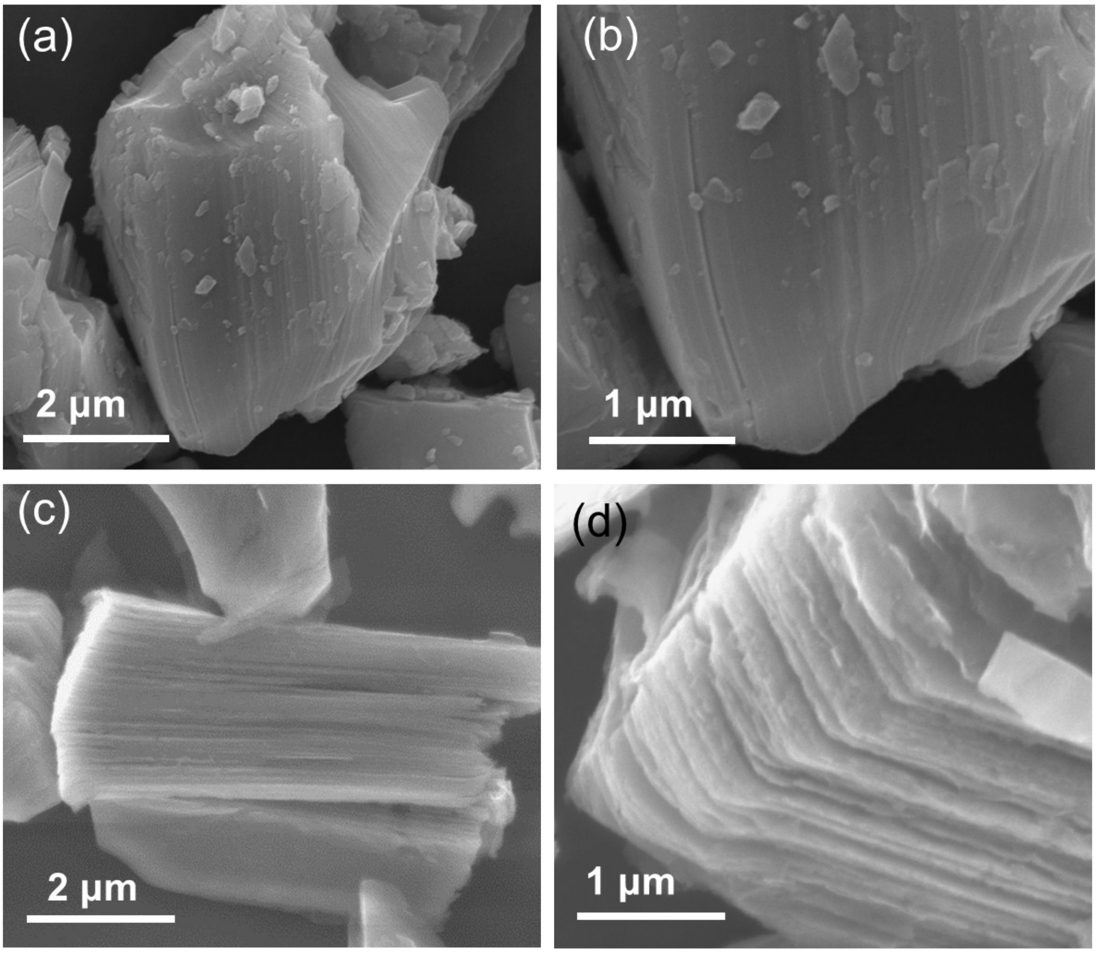

Fig. S3. SEM images of (a, b) Ti_3SiC_2, (c-d) $Ti_3C_2(H_2O_2\text{-}40)$.

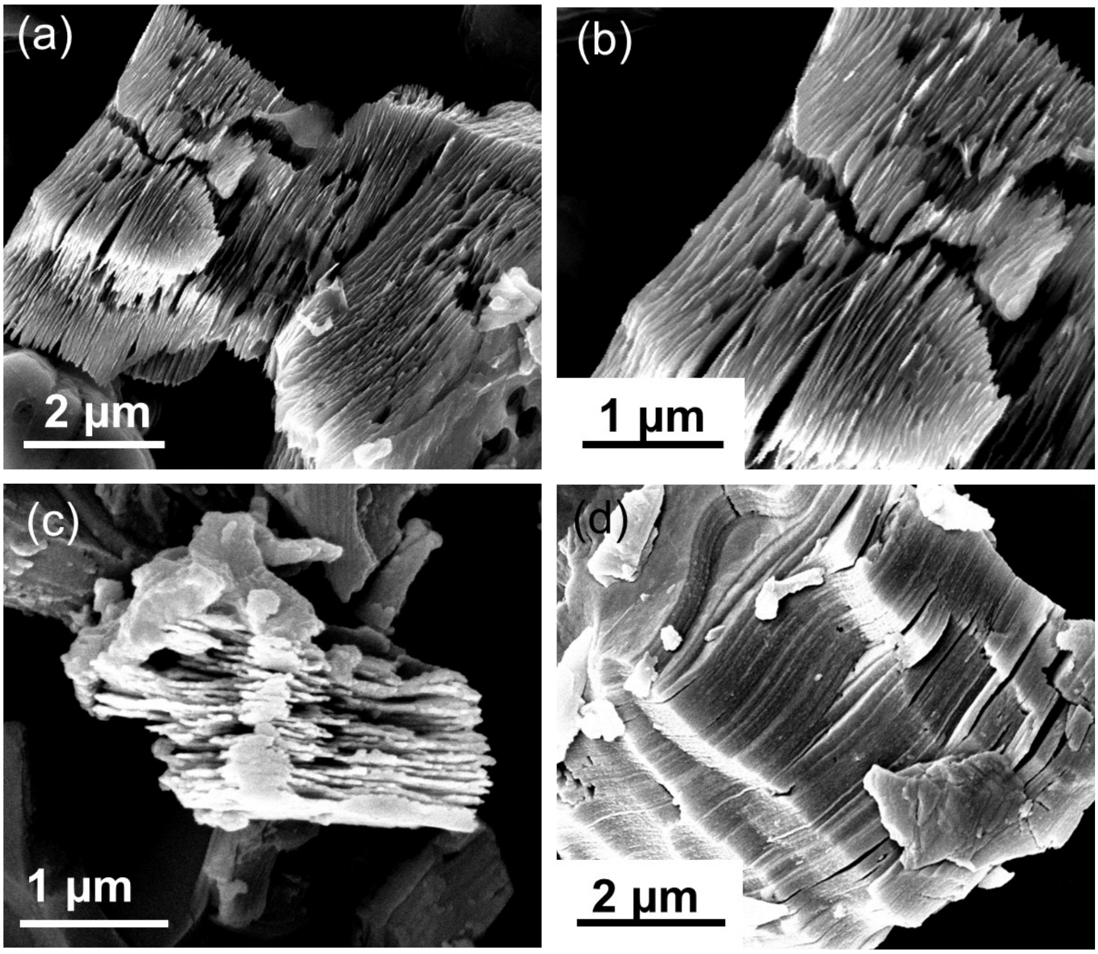

Fig. S4. SEM images of (a, b) $Ti_3C_2(H_2O_2\text{-}70)$, (c) Ti_3C_2 (HNO_3-40) and (d) Ti_3C_2 (AR-RT).

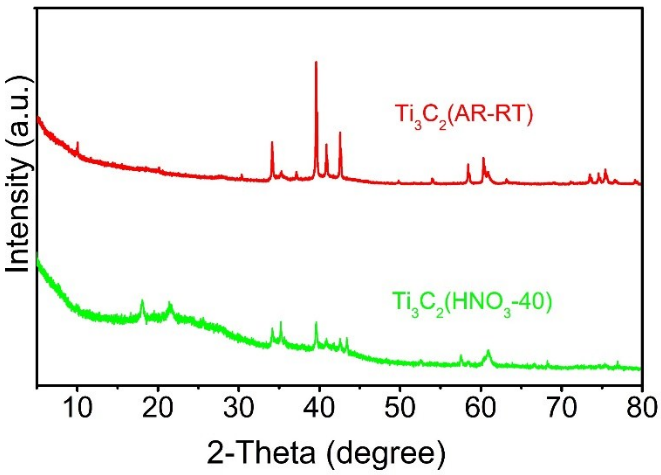

Fig. S5. XRD patterns of Ti_3C_2(HNO_3-40) and Ti_3C_2 (AR-RT).

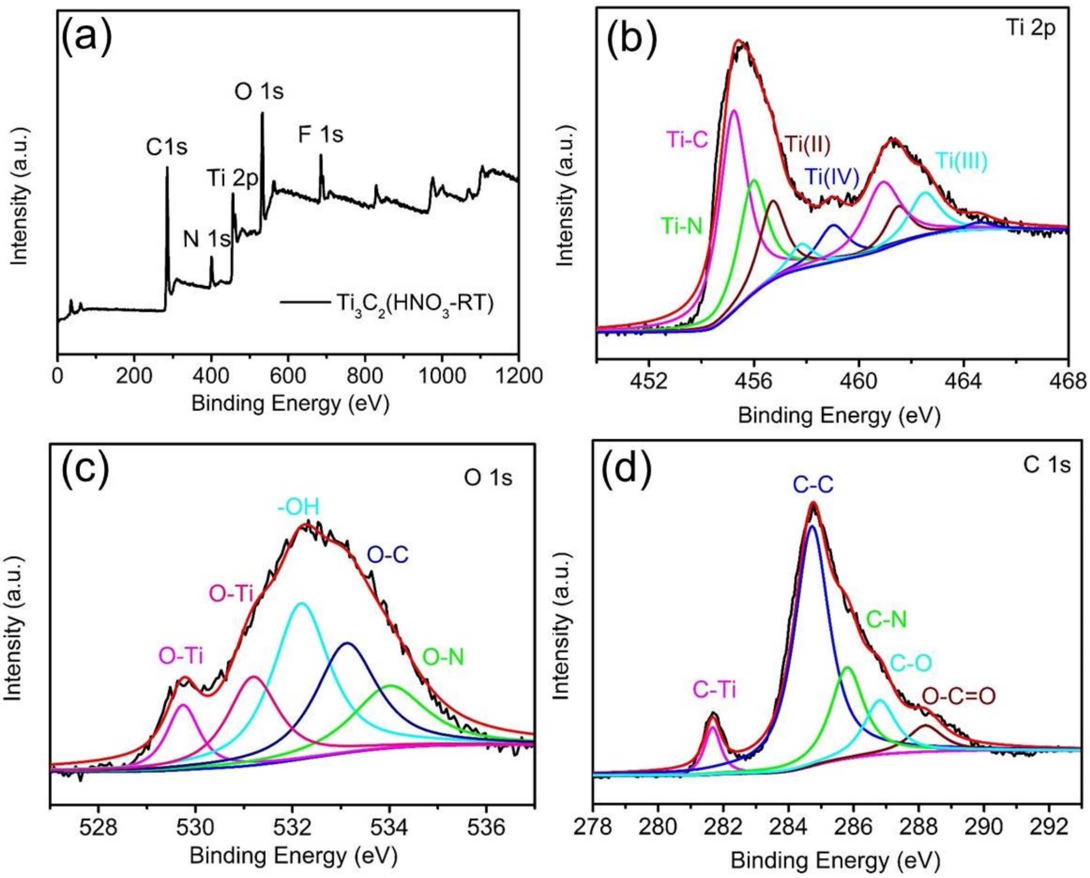

Fig. S6. (a) XPS survey scan of Ti_3C_2(HNO_3-RT), and high-resolution XPS spectra of (b) Ti 2p, (c) O 1s and (d) C 1s.

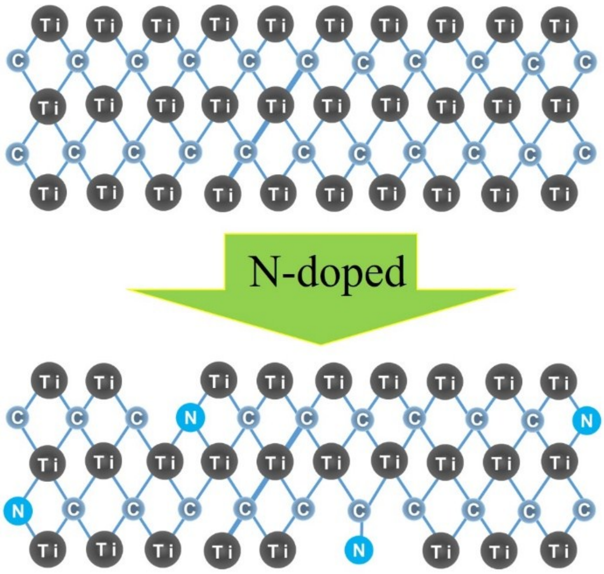

Fig. S7. Schematic diagram for the N doping process.

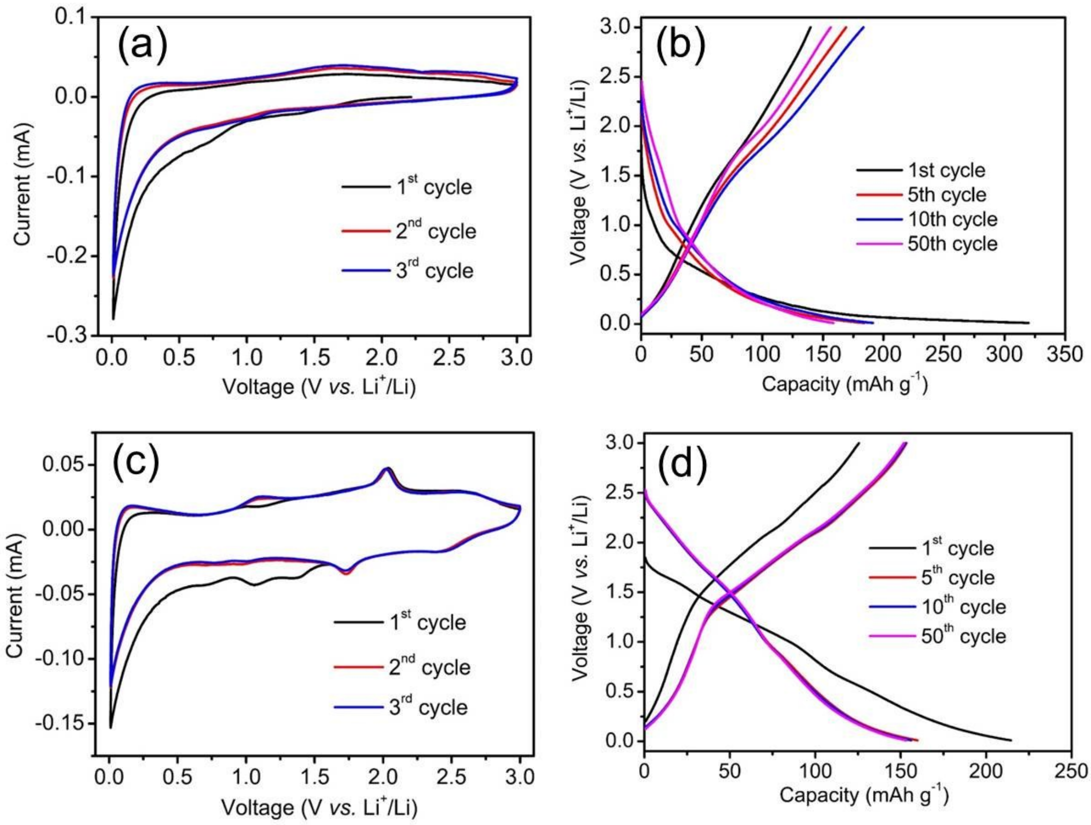

Fig. S8. Cyclic voltammogram of the Ti_3C_2(HNO_3-RT) (a) and Ti_3C_2@TiO_2(H_2O_2-60) (c) electrodes in the initial 3 cycles at a rate of 0.1 mV s^{-1}; Charge/discharge curves of the Ti_3C_2(HNO_3-RT) (b) and Ti_3C_2@TiO_2(H_2O_2-60) (d) electrodes at different cycles, respectively.

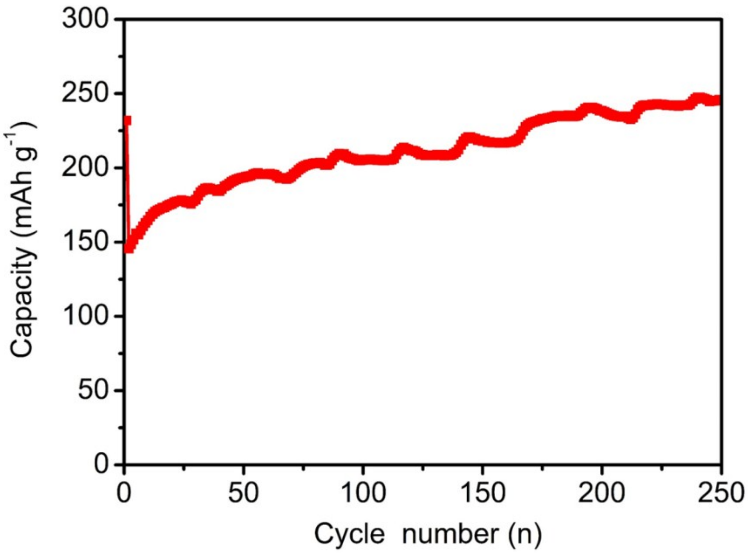

Fig. S9. Discharge capacity of N-doped Ti_3C_2@TiO_2(HNO_3-RT) electrodes at 500 mA g^{-1}.

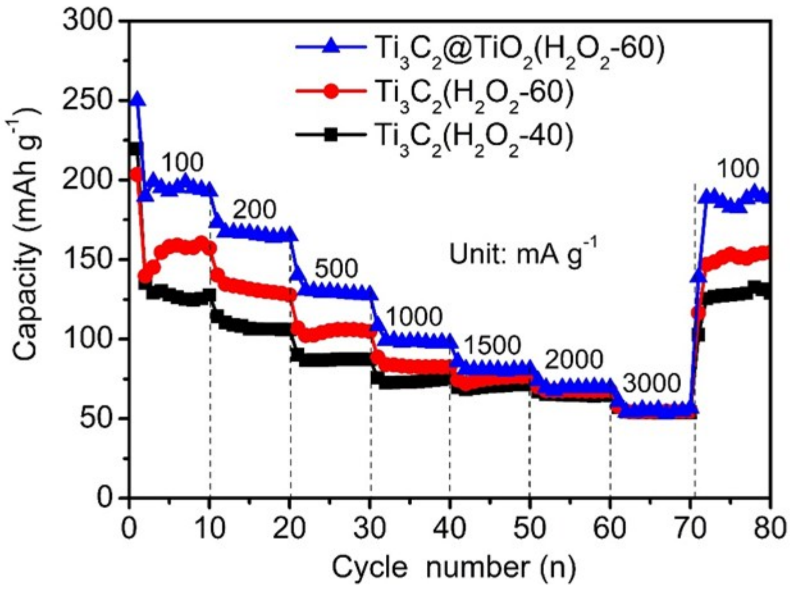

Fig. S10. Rate capability of the Ti_3C_2 and $Ti_3C_2@TiO_2$ electrodes (H_2O_2 as oxidant), respectively.

Compared with the rate capabilities of $Ti_3C_2(H_2O_2\text{-}40)$ and $Ti_3C_2(H_2O_2\text{-}60)$ electrodes, the rate capacity of $Ti_3C_2@TiO_2(H_2O_2\text{-}60)$ is higher and the discharge specific capacities are 195, 166, 129, 98, 80, 69 and 56 mA h g^{-1} at 100, 200, 500, 1000, 1500, 2000 and 3000 mA g^{-1}, respectively.

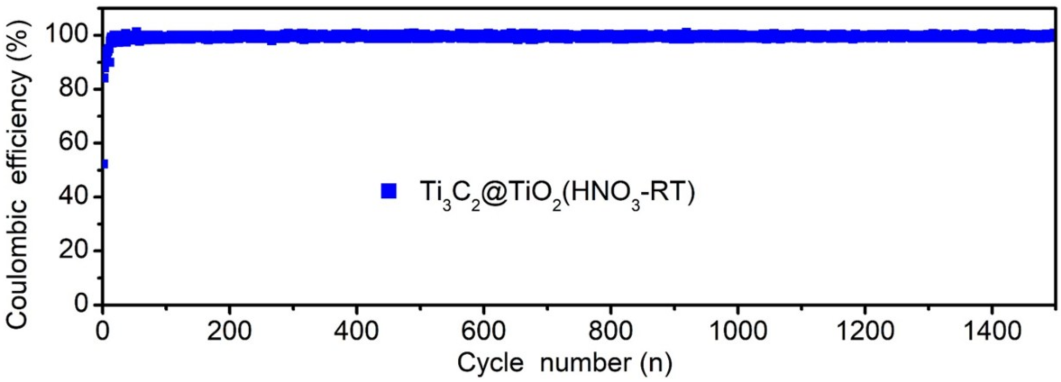

Fig. S11. The coulombic efficiency of N-doped Ti_3C_2@TiO_2(HNO_3-RT) electrode at 2000 mA g^{-1}.

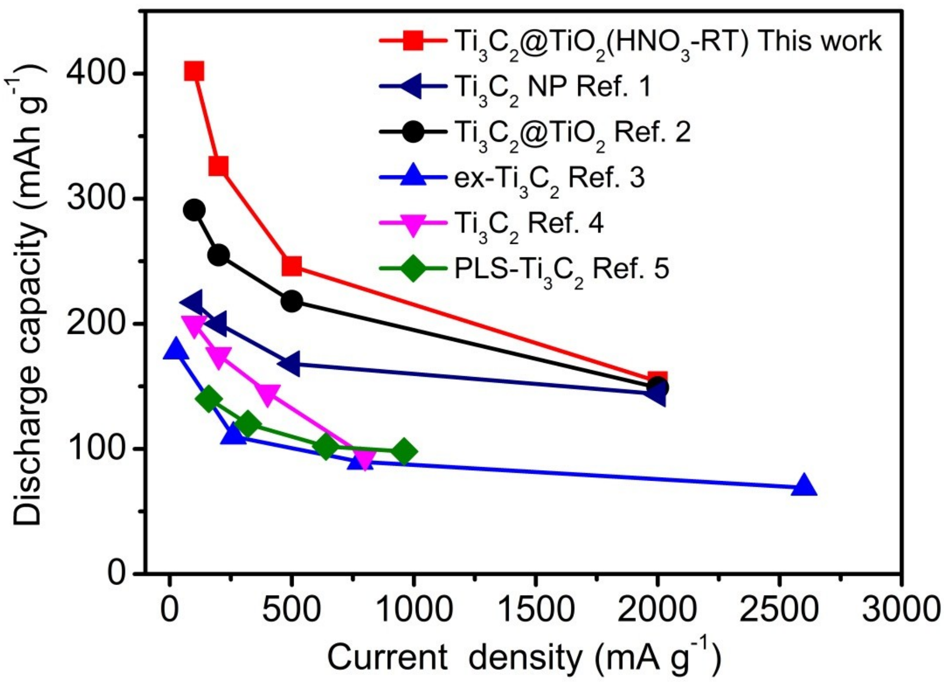

Fig. S12. Comparisons in the rate capabilities between this work and other Ti_3C_2-based electrodes.

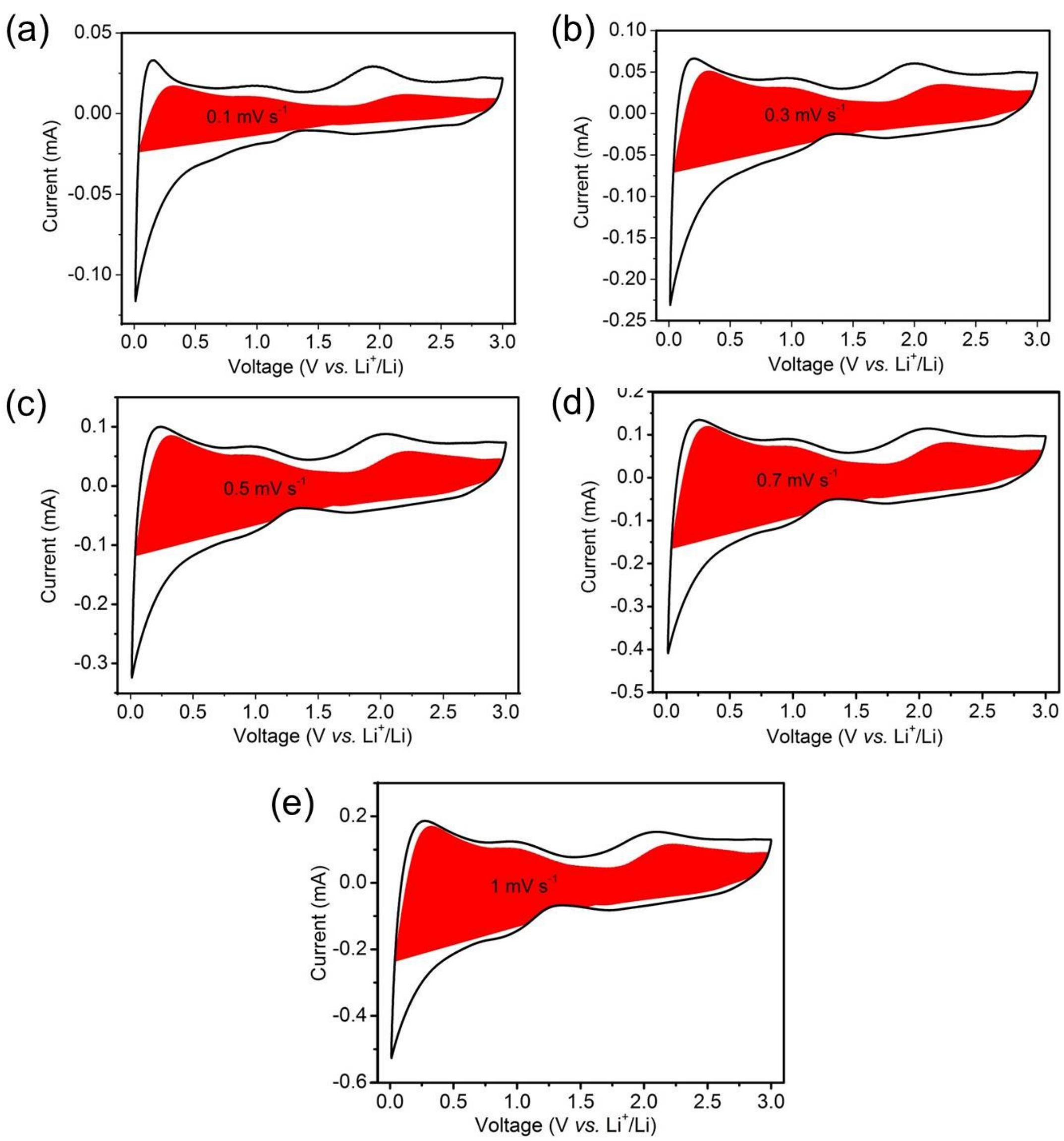

Fig. S13. CV profiles with shaded portion showing the capacitive contribution at 0.1, 0.3, 0.5, 0.7 and 1 mV s^{-1}.

Table S1 Different preparation conditions and labeling of Ti_3C_2 and $Ti_3C_2@TiO_2$, respectively.

MAX	Etchant	T (^oC)	Time (h)	Hydrothermal	Product record
Ti_3SiC_2	HF	40	48	No	Ti_3SiC_2(HF-40)
Ti_3SiC_2	H_2O_2+HF	40	48	No	Ti_3C_2(H_2O_2-40)
Ti_3SiC_2	H_2O_2+HF	60	48	No	Ti_3C_2(H_2O_2-60)
Ti_3SiC_2	H_2O_2+HF	70	48	No	Ti_3C_2(H_2O_2-70)
Ti_3SiC_2	H_2O_2+HF	60	48	Yes	$Ti_3C_2@TiO_2$(H_2O_2-60)
Ti_3SiC_2	HNO_3+HF	Room temperature	40	No	Ti_3C_2(HNO_3-RT)
Ti_3SiC_2	HNO_3+HF	40	40	No	Ti_3C_2(HNO_3-40)
Ti_3SiC_2	HNO_3+HF	Room temperature	40	Yes	$Ti_3C_2@TiO_2$(HNO_3-RT)
Ti_3SiC_2	AR+HF	Room temperature	40	No	Ti_3C_2(AR-RT)

Table S2 Summary of the electrochemical performances of Ti_3C_2-based electrodes at various current densities in LIBs.

Electrode material	Current density (mA g^{-1})	Cycle number (n)	Capacity (mA h g^{-1})	Ref.
MXene nanosheets	1000	500	139	1
Ti_3C_2	200	500	203	2
Ti_3C_2@TiO_2	200	500	267	2
Pure Mo_2TiC_2Tx	100	100	52	6
Ti_3C_2 film	1000	1000	70	7
Flash-air oxidized $Ti_3C_2T_x$	320	300	155	8
SnO_2/MXene	100	50	258	9
SHS-Ti_3C_2	1C	100	53	10
PLS-Ti_3C_2	1C	100	87	10
Ti_3C_2	100	100	108	11
CoO@Ti_3C_2	100	100	324	11
Ti_3C_2	125	1000	135	12
Ti_3C_2	100	100	125	13
Ti_3C_2	100	50	91	14
Ti_3C_2	100	200	82	15
Ti_3C_2@TiO_2(H_2O_2-60)	2000	1500	106	This work
Ti_3C_2(HNO_3-RT)	200	250	201	This work
Ti_3C_2@TiO_2(HNO_3-RT)	200	250	339	This work
Ti_3C_2@TiO_2(HNO_3-RT)	500	250	246	This work
Ti_3C_2@TiO_2(HNO_3-RT)	2000	1500	154	This work

References

[1] Y.T. Liu, P. Zhang, N. Sun, B. Anasori, Q.Z. Zhu, H. Liu, Y. Gogotsi and B. Xu, Self-Assembly of Transition Metal Oxide Nanostructures on MXene Nanosheets for Fast and Stable Lithium Storage, *Adv. Mater.*, 2018, **30**, 1707334.

[2] C. Yang, Y. Liu, X. Sun, Y.R. Zhang, L.R. Hou, Q.G. Zhang and C.Z. Yuan, *In-situ* construction of hierarchical accordion-like TiO_2-Ti_3C_2 nanohybrid as anode material for lithium and sodium ion batteries, *Electrochim. Acta*, 2018, **271**, 165-172.

[3] D. Sun, M. Wang, Z. Li, G. Fan, L. Z. Fan, A. Zhou, Two-dimensional Ti_3C_2 as anode material for Li-ion batteries, *Electrochem. Commun.*, 2014, 47, 80-83.

[4] X.F. Wang, X. Shen, Y.R. Gao, Z. Wang, R. Yu and L. Chen, Atomic-Scale Recognition of Surface Structure and Intercalation Mechanism of Ti_3C_2X, *J. Am. Chem. Soc.*, 2015, 137, 2715-2721.

[5] F.Y. Kong, X.D. He, Q.Q. Liu, X.X. Qi, Y.T. Zheng, Effect of Ti_3AlC_2 precursor on the electrochemical properties of the resulting MXene Ti3C2 for Li-ion batteries, *Ceram. Int.*, 2018, 44, 11591-11596.

[6] C. Chen, X. Xie, B. Anasori, A. Sarycheva, T. Makaryan, M. Zhao, P. Urbankowski, L. Miao, J. Jiang and Y. Gogotsi, MoS_2-on-MXene Heterostructures as Highly Reversible Anode Materials for Lithium-Ion Batteries, *Angew. Chem. Int. Edit.*, 2018, **57**, 1846-1850.

[7] Z. Ma, X. Zhou, W. Deng, D. Lei and Z. Liu, 3D Porous MXene (Ti_3C_2)/Reduced Graphene Oxide Hybrid Films for Advanced Lithium Storage, *ACS Appl. Mater. Interfaces*, 2018, **10**, 3634-3643.

[8] M. Naguib, O. Mashtalir, M.R. Lukatskaya, B. Dyatkin, C.F. Zhang, V. Presser, Y. Gogotsi and M.W. Barsoum, One-step synthesis of nanocrystalline transition metal oxides on thin sheets of disordered graphitic carbon by oxidation of MXenes, *Chem. Commun.*, 2014, **50**, 7420-7423.

[9] B. Ahmed, D.H. Anjum, Y. Gogotsi and H.N. Alshareef, Atomic layer deposition of SnO_2 on MXene for Li-ion battery anodes, *Nano Energy*, 2017, **34**, 249-256.

[10] F. Kong, Q.Q. Liu, X.X. Qi, Y.T. Zheng, R.G. Wang and Y.L. Bai, Effect of

Ti_3AlC_2 precursor on the electrochemical properties of the resulting MXene Ti_3C_2 for Li-ion batteries, *Ceram. Int.*, 2018, **44**, 11591-11596.

[11] X.L. Li, Y. Fang, W.J. Lv, F. Wang, Y. Liu and H. Liu, Hydrothermal preparation of CoO/Ti_3C_2 composite material for lithium-ion batteries with enhanced electrochemical performance, *J. Electroanal. Chem.*, 2018, **817**, 1-8.

[12] Y.S. Wang, Y.Y. Li, Z.P. Qiu, X.Z. Wu, P.F. Zhou, T. Zhou, J.P. Zhao, Z.C. Miao and S.P. Zhuo, Fe_3O_4@Ti_3C_2 MXene hybrids with ultrahigh volumetric capacity as an anode material for lithium-ion batteries, *J. Mater. Chem. A*, 2018, **6**, 11189-11197.

[13] J. Luo, W. Zhang, H. Yuan, C. Jin, L. Zhang, H. Huang, C. Liang, Y. Xia, J. Zhang, Y. Gan and X. Tao, Pillared Structure Design of MXene with Ultralarge Interlayer Spacing for High-Performance Lithium-Ion Capacitors, *ACS Nano*, 2017, **11**, 2459-2469.

[14] J. Luo, X. Tao, J. Zhang, Y. Xia, H. Huang, L. Zhang, Y. Gan, C. Liang and W. Zhang, Sn^{4+} Ion Decorated Highly Conductive Ti_3C_2 MXene: Promising Lithium-Ion Anodes with Enhanced Volumetric Capacity and Cyclic Performance, *ACS Nano*, 2016, **10**, 2491-2499.

[15] F. Wang, Z.J. Wang, J.F. Zhu, H.B. Yang, X.J. Chen, L. Wang and C.H. Yang, Facile synthesis SnO_2 nanoparticle-modified Ti_3C_2 MXene nanocomposites for enhanced lithium storage application, *J. Mater. Sci.*, 2017, **52**, 3556-3565.